International Journal of Heat and Mass Transfer 143 (2019) 118484

Contents lists available at ScienceDirect

International Journal of Heat and Mass Transfer

journal homepage: www.elsevier.com/locate/ijhmt

Heat transfer enhancement of air-cooled heat sink channel using a piezoelectric synthetic jet array

Taiho Yeom [a], Longzhong Huang [b], Min Zhang [c], Terrence Simon [b], Tianhong Cui [b,*]

[a] Department of Mechanical Engineering, University of Mississippi, University, MS 38677, USA
[b] Department of Mechanical Engineering, University of Minnesota, Minneapolis, MN 55455, USA
[c] Graduate School at Shenzhen, Tsinghua University, Shenzhen 518055, China

ARTICLE INFO

Article history:
Received 6 April 2019
Received in revised form 22 July 2019
Accepted 25 July 2019
Available online 12 August 2019

Keywords:
Synthetic jet array
Electronics cooling
Heat sink
Piezoelectricity
Heat transfer enhancement

ABSTRACT

In the last decade, active devices, such as synthetic jets have been intensively studied for electronics cooling. The present study experimentally and computationally investigates heat transfer performance of synthetic jet arrays used in heat sink channels. The heat sink of the present study consists of multiple flow channels that are parallel to one another. The channel walls behave like fins in that their tops are exposed to the flow. The jets are designed to impinge on the tops and sides of those fins to augment heat transfer. The current study employs a single channel of the heat sink to investigate heat transfer augmentation performance by the jets. The oscillating diaphragms that create the jets are driven by a piezo-bow operating at its second resonant vibrational mode to generate a large oscillatory displacement at a high working frequency. The frequency for this study is 1240 Hz and the measured displacement of the jet-driving diaphragm is 0.5 mm. The corresponding peak velocity of each jet is around 45 m/s and the total power consumption is 1.6 W when operating with 20 jets. Heat transfer experiments using jet arrays of different jet orifice configurations are conducted in a single narrow channel that represents one of the channels of a multi-channel heat sink. With a through-flow velocity of 14.7 m/s driven by a centrifugal fan, the synthetic jet arrays with square orifices achieve 9.3% enhancement on heat transfer coefficient averaged over the entire fin (channel wall) surface, compared to the value for a case with through-flow only. When the channel through-flow velocity decreases to 8 m/s spatially-averaged heat transfer enhancement by the jets is 21.7%; again, averaged over the entire fin (channel wall) surface. In a computational study, the jet diaphragm movement is realized with a dynamic mesh available within the commercial software package ANSYS Fluent. Computed surface-average Nusselt numbers show good agreement with the experimental data, differing by no more than 10%. The numerical study was performed to quantify the effects of system parameters, such as the jet and channel flow rates and orifice-to-fin-surface distance, on heat transfer performance over different sections of the channel (fin) wall. According to the results of the numerical study, the synthetic jets have a strong cooling effect on the channel wall tip region, the nearest surface to the jet orifice, and a weaker effect on the channel side surfaces. It is found that the synthetic jet can enhance locally-averaged heat transfer coefficients at the fin tip by up to 413%, compared to a case with cooling by channel through-flow only.

1. Introduction

Efficient heat removal from compact and powerful electronics systems requires effective thermal management techniques A variety of cooling methods has been proposed and developed to meet the rising requirements. Liquid cooling, such as single phase [1–5], nanofluids [6,7], multi-phase flow [8–12], direct spray [13,14], and pool boiling [15–17], can provide significant cooling capability. However, these methods need additional apparatus, such as reservoirs, pumps, piping systems, nozzles, spray systems, and others that make liquid cooling expensive and complex. Reliability issues related to leakage and corrosion are drawbacks. Thus, there is support for further extending the capability of air cooling beyond the current capacity. A traditional method of air cooling for electronics is to use the combination of a heat sink and an external fan for through-flow. A finned heat sink increases the surface area for heat transfer. This is done by shortening the channel walls and exposing their tips to the flow. Much effort has been expended to optimize and advance forced-convection heat sink technology [18–23].

* Corresponding author.
E-mail address: cuixx006@me.umn.edu (T. Cui).

https://doi.org/10.1016/j.ijheatmasstransfer.2019.118484
0017-9310/

Nomenclature

A_s	convective surface area (m^2)
A_c	cross sectional area (m^2)
c_p	specific heat (J/kg)
d_h	hydraulic diameter of orifice (m)
D_h	hydraulic diameter of the channel (m)
f	frequency of diaphragm movement (Hz)
h	average heat transfer coefficient (W/m^2 K)
k_c	thermal conductivity of copper (W/m K)
k_f	thermal conductivity of fluid (W/m K)
L	length of the fin (m)
Nu	Nusselt number
Pr	Prandtl number
Q	heater power input (W)
$\dot{Q}$	volume flow rate (m^3/s)
R	fin tip radius (m)
Re	Reynolds number
*Re*_channel	(Reynolds number of channel flow) = $\rho U D_h/\mu$
*Re*_jet	Reynolds number of synthetic jet flow = $\rho V_j d_h/\mu$
S	the spacing between two jets (m)
T	temperature (K)
U	average velocity of channel flow (m/s)
V_j	synthetic jet peak velocity (m/s)
W	width of the fin (m)
X	channel length
z	distance between orifice and fin tip (m)

Subscripts

air_in	channel inlet air
air_out	channel outlet air
fin_in	fin in the inlet region
fin_out	fin in the outlet region
jet	synthetic jet flow
channel	channel flow
LMTD	log mean temperature difference

Greek symbols

μ	dynamic viscosity of fluid (N s/m^2)
ν	kinematic viscosity of fluid (m^2/s)
ρ	density of fluid (kg/m^3)

However, present electronics heat transfer requires a more compact, higher-power system. Thus, various active air-cooling methods have been proposed over the last decade. A piezo fan is a promising device for cooling of small regions of electronics [24–28]. The piezo fan consists of a flexible shim attached to a piezoelectric patch to generate a flapping motion at the shim tip, when oscillated. Air currents made from the flapping motion are utilized to convectively cool the heated surface. Some researchers investigated a corona wind generated by a large driving voltage [29,30] as an active cooling technique. Yeom et al. [31–33] developed a piezoelectric translational agitator to incorporate into a heat sink system, leading to significant enhancement on cooling performance.

The synthetic jet is an active air-cooling technology that has gained attention in the past decade. In its basic configuration, shown in Fig. 1, a synthetic jet is driven by a cavity having an orifice at one end. The jet is driven by an oscillating diaphragm at the opposite end of the cavity. The diaphragm produces unsteady air flow into and out of the cavity, forming pairs of vortex rings near the exit from the orifice that can enhance heat transfer from surfaces in their path.

Several studies have been performed on utilizing synthetic jet impingement for cooling. Chaudhari et al. [34] experimentally investigated heat transfer characteristics of synthetic jet impingement on a heated flat surface with various orifice diameters, axial distances between orifice and heated surface, and orifice plate designs. Their synthetic jet achieved a maximum average heat transfer coefficient of 143 W/m^2 K at an operating frequency of 250 Hz with an orifice of 8 mm diameter. They found that the average heat transfer coefficient increased to a certain level and then decreased with increases of axial distance between the orifice plate and the heated surface. Chaudhari et al. [35] investigated effects on synthetic jet cooling with various orifice shapes using circular, square, rectangular, and slit geometries with different aspect ratios while keeping the same hydraulic diameter. The results in terms of average Nusselt numbers showed that the case with a square orifice generated the best heat transfer performance. Pavlova and Amitay [36] studied cooling performance over a constant heat flux surface of a synthetic jet driven by a piezoelectrically-driven disk with a diameter of 30 mm. The results indicated that a high operating frequency of 1.2 kHz provided better cooling performance at smaller jet-to-surface distances while a low operating frequency of 420 Hz was more effective at larger separation distances. The results further showed that the synthetic jet was three times as effective as a continuous jet operating at the same mean flow speed Reynolds number. Garg et al. [37] fabricated a synthetic jet that can generate a maximum velocity of 90 m/s at an operating frequency of 4.4 kHz. The orifice shape was rectangular with a hydraulic diameter of 0.85 mm. They found that the cooling effectiveness was not very sensitive to jet oscillator driving voltage,

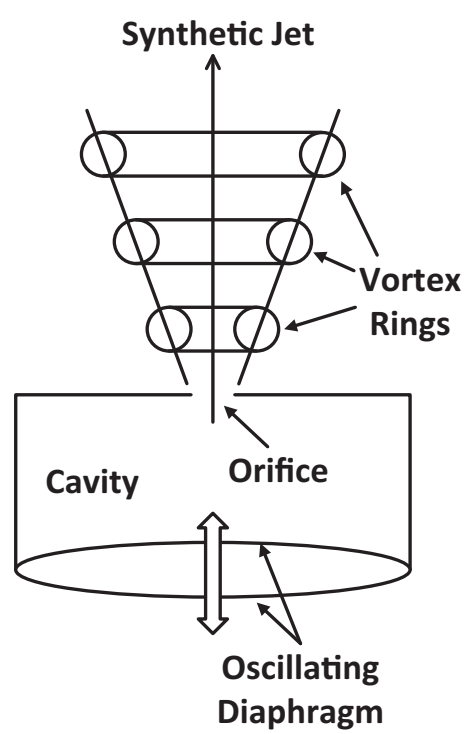

Fig. 1. A basic configuration of a synthetic jet.

which would relate to diaphragm displacement. The synthetic jet achieved a maximum average heat transfer coefficient of 240 W/m^2 K, which is about 10 times that of natural convective cooling. Utturkar et al. [38] conducted experimental and numerical studies on heat transfer characteristics of pulsating jets with different jet-to-surface distances and flow orientations. The maximum velocity of pulsation reached up to 45 m/s at an operating frequency of 4.5 kHz. The Coefficient of Performance (COP), defined as heat transfer per driving power, was measured to be as high as 10, indicating that cooling by a synthetic jet is efficient. Numerical simulation results agreed well with experimental data for average heat transfer coefficients, within 5%. The results indicated that a non-perpendicular jet orientation can be as efficient as a perpendicular jet orientation, if properly optimized. Arik [39] performed cooling characterization of a high-frequency synthetic jet by measuring the local and global heat transfer coefficients over 6.25 mm, 12.7 mm, 25.4 mm and 50.8 mm square heater surfaces. The synthetic jet used a square orifice with a hydraulic diameter of 1.0 mm and operated at 4.5 kHz. The measured global heat transfer coefficients over the heated surface were 10 times those of natural convection when using the smallest heater size of 6.25 mm. The results showed that the effects of jet-to-surface spacing on heat transfer enhancement depend on the size of the heater. The smaller heaters of 6.25 mm and 12.7 mm showed strong dependency on orifice-to-surface spacing. In addition to the above experimental studies, many researchers focused on numerical investigations of heat transfer enhancement by synthetic jets. Jagannatha et al. [40] performed a 2-D numerical study on unsteady characteristics of synthetic jets using FLUENT. The oscillating diaphragm was set as a moving boundary and the Shear-Stress-Transport (SST) k-ω model was used for the turbulence closure model. The results indicate that heat transfer performance by the synthetic jet is highly related to diaphragm oscillation amplitude and operating frequency. The ranges of operational frequency and diaphragm amplitude were 250–1000 Hz and 0.5–2.0 mm, respectively. The corresponding Reynolds numbers calculated with a characteristics velocity defined by Smith and Glezer [41] ranged from 162 to 2781. The average Nusselt numbers were calculated as 20–120 times those of natural convection under the same operational conditions. They also found that synthetic jets outperformed continuous jets of the same mean speed Reynolds number. Chandratilleke et al. [42] used unsteady Reynolds-Averaged Navier-Stokes (RANS) equations with the SST k-ω turbulence closure model to numerically investigate heat transfer performance of a synthetic jet-microchannel hybrid heat sink system. The operating frequency of the synthetic jet was 10 kHz and the diaphragm amplitude ranged up to 100 μm. It was found that the micro heat sink coupled with synthetic jet cooling achieved 60 times the average heat transfer rate of pure natural convection. Behera et al. [43] numerically investigated heat transfer performance of impinging jets in terms of time-averaged local Nusselt number. The jet used sinusoidal and square wave pulsations of the flow with mean Reynolds numbers in the range of 5130–8560. The operating frequency ranged between 25 and 400 Hz. The heated wall had a uniform and constant heat flux condition. The results indicated that a jet driven by a sine wave was superior to the square wave for heat transfer enhancement. In addition, they concluded that the amplitude had a larger impact on heat transfer than the frequency. Erbas and Baysal [44] performed 2-D numerical simulations of channel flow in conjunction with synthetic jet impingement over a microchip generating a constant heat flux. They examined the effects on average heat transfer coefficient of orifice throat geometry, jet spacing, phase offset of multiple jet operation, and downstream location of the synthetic jet in the channel. The results showed that a maximum heat transfer coefficient of 268 W/m^2 K was achieved when the single synthetic jet was centered on the microchip. Among various throat geometries tested, a nozzle-like throat was shown to help increase average heat transfer rate from the chip surface. In addition, providing a 180-degree phase difference between two jets resulted in better cooling performance than with two synchronized jets. Terzis et al. [45] experimentally investigated staggering effects of synthetic jet impingement for a gas turbine blade wall with a narrow internal channel. Engine-representative Reynolds numbers of between 11,100 and 86,000 were considered with different impingement hole arrangements, inline and staggered. Heat transfer performance was measured using the transient liquid crystal method. The results indicated that the separation distance of the staggered jets has a small effect on average heat transfer coefficient on the target wall and heat transfer performance was reduced with increased jet-to-wall separation distance. The inline configuration showed the best heat transfer performance. Additional studies showing detailed heat transfer characteristics of similar experimental configurations, engine Reynolds numbers, number of jets, and choice of measurement technique were conducted by Terzis et al. [46]. It was confirmed, again, that jet staggering reduced heat transfer performance on the target wall.

In the current study, heat transfer enhancement by a synthetic jet array impinging on an electronics cooling heat sink channel is investigated by experimental and numerical techniques. The heat transfer test section is fabricated to simulate a single heat sink channel with channel flow and synthetic jet impingement on the channel wall. A PZT stack actuator with a bow-type structure [47] for amplification is used to drive an array of synthetic jets. The jet peak velocity reached around 45 m/s. Heat transfer performance features of the synthetic jet arrays with five different orifice shapes are evaluated. The results indicate that a square orifice provides the best heat transfer performance. A maximum heat transfer enhancement of 21.7% is achieved with the square orifice jet array when operating with 8 m/s channel through-flow. A numerical simulation is conducted using the ANSYS Fluent software package and its results are validated with experimental results. An investigation on heat transfer performance under various operational conditions of synthetic jet impingement is conducted by numerical simulation.

2. Experimental study

2.1. Piezoelectric synthetic jet arrays

In the current study, the synthetic jet arrays are designed to impinge air jets onto the tip portion of the fins of an induced-flow heat sink. This study isolates a single channel. Details regarding active heat sink technology can be found in a previous report [48] in which a synthetic jet array was employed as one of the components for enhancing thermal performance of the air-cooled heat sink. In this previous study on the active heat sink technology, the operational conditions of the synthetic jet arrays were fixed and its relative cooling performance was compared to other components of a piezoelectric translational agitator and micro pin fins. In the current study, synthetic jet operation over a broad range of conditions was tested to investigate the cooling performance of jets within the active heat sink environment. Fig. 2 shows the structure of the synthetic jet actuator consisting of a cavity with an oscillating piston at one side and an orifice array at the opposite side. A flexible latex diaphragm is used to connect the piston to the cavity. The piston is driven by the piezo-bow actuator, shown in Fig. 2(b). The bow structure is cut by the wire EDM from 5160 spring steel. The PZT stack actuator within the bow structure expands a few micrometers in length in an oscillating fashion with a sinusoidal applied voltage. The bow structure amplifies this small displacement in an orthogonal direction to the millimeter displace-

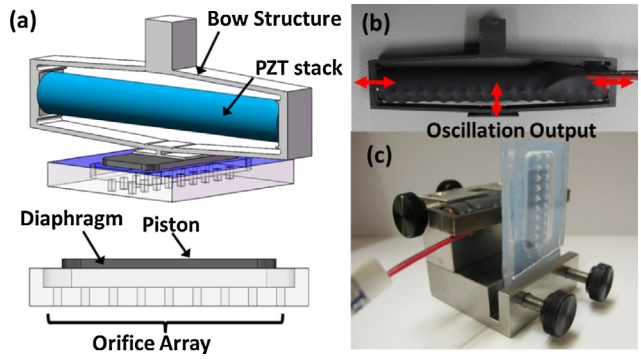

Fig. 2. (a) Schematic of synthetic jet array driven by piezo-bow with piston-diaphragm structure. (b) Piezo stack and bow structure assembly, (c) Piezoelectric synthetic jet array module.

ment range, when driven at its resonant frequency. This oscillating motion is transferred to the piston and drives the synthetic jets' flow through the orifices. The unsteady flow generates unsteady vortex rings that travel with the jet flow. The piston that drives the diaphragm is made of a 14 mm × 26 mm × 1 mm carbon fiber plate. Five different orifice shapes, including circular, split-circular, square, double-slot, and inclined, were tested to find an orifice configuration for maximizing heat transfer enhancement on the heat sink channel (Fig. 3).

The 20 split-circular orifice configuration is intended to impinge jets on the side surfaces of the heat sink fin. The orifice diameter is adjusted to match the total orifice area similar to that of the 20 circular orifice configuration. The square type has a slightly larger total orifice area than two circular type. The inclined type has the orifices and their nozzles are inclined 60 degrees towards the streamwise direction hoping to provide additional momentum to the channel through-flow for enhancing channel heat transfer. However, it has only 12 orifices and the smallest total orifice area due to space limitation. The calculated total areas of different orifice types are summarized in Table 1.

The vibration characteristics of the synthetic jet were measured by a Polytec PSV-400 scanning laser Doppler Vibrometer (LDV). The vibration measurement of the piston was taken by passing a laser beam from the LDV through the orifice openings. The operating frequency of the synthetic jets driven by the piezo-bow actuator was measured to be 1240 Hz. The vibration measurement results show that a typical peak-to-peak displacement of the piston within the jet cavity is around 0.5 mm at a driving voltage of 100 VAC, about 30% lower than the 0.735 mm measured without the jet cavity attached to the piezo-bow actuator. The velocities of the jets were measured using hot-film anemometry. The small size of the synthetic jet orifices required use of a miniature hot-film

Table 1
Total orifice area for different orifice configurations.

Orifice type	Total orifice area (mm^2)
20 Circular	15.7
20 Split-circular	15.4
20 Square	16.2
Double-slot	28.0
12 Inclined	9.4

probe (1277-10A, TSI, USA) with an effective length of 0.25 mm. The hot-film probe was centered on the orifice and located 3 mm away from the orifice exit plane. Fig. 4 shows the instantaneous velocity measurement of the jet from a 0.9 mm × 0.9 mm square orifice array operating at 1240 Hz and 100 VAC as it is expected to show the maximum jet velocity among the five different orifice types. The orifices are numbered from the left row (#1) to the right row (#10), as shown in Fig. 4(a). The average peak velocities range over 43–45 m/s, depending on position of the orifice on the orifice plate. The instantaneous maximum jet velocity from the #3 orifice (Fig. 4(b)) reached 47 m/s. The power consumption of the synthetic jet was obtained by integrating and averaging the instantaneous product of current and voltage across the PZT stack actuator over the period of measurement. A standard precision resistor of 0.2 Ω was placed in the driving circuit of the PZT and the current was measured using an oscilloscope. The measured power consumption of the jet actuator working under these conditions was 1.6 W.

2.2. Single-channel heat transfer test set up

The single channel heat sink unit used for the heat transfer experiments with the synthetic jet array is shown in Fig. 5. A long copper block is used to conduct thermal energy from the cartridge heater attached at the bottom surface to the heat sink channel at the other end. Air flows into the channel from both ends, turns 90°, and exits upward to a 20 mm × 4.5 mm opening in the center of the channel. The heated air from the test section flows into the piping system instrumented with a volumetric flow meter (Sierra, Model 826-NX-OV1-PV1-V1), a valve and a vacuum pump. The channel is made by two half-fins machined from a copper block. Details of the heat sink channel are shown in Fig. 6. The height of the half-fin is 16.5 mm. The width of the channel is 3.4 mm. The entire length of the channel is 89 mm between the two inlets. However, the actual channel length (X) to calculate flow and heat transfer characteristics in this paper is 44.5 mm as the flow exits in the center of the heat sink channel. The half-fin has the thickness of 0.8 mm. The remaining half of the fin is made of plastic insulation. Two synthetic jet assemblies and a discharge adaptor cover the top of the channel, as shown in Fig. 5. The orifice centers are

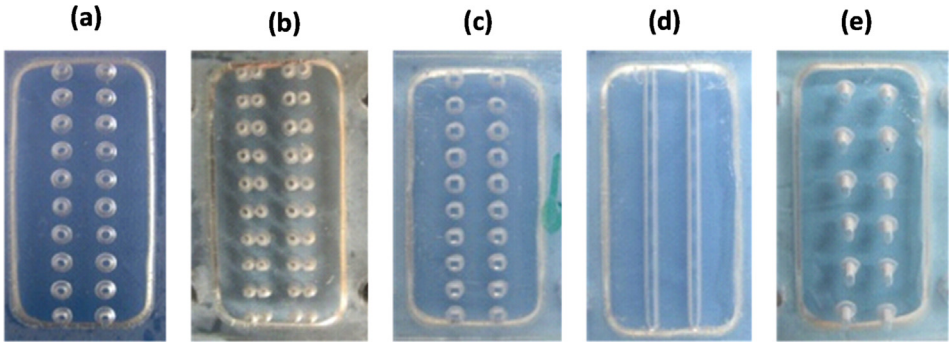

Fig. 3. Various orifice types: (a) 20 Circular (∅ = 1 mm), (b) 20 Split-circular (∅ = 0.7 mm), (c) 20 Square (0.9 mm × 0.9 mm), (d) Double-slot (0.5 mm × 28 mm), (e) 12 Inclined (∅ = 1 mm, 60°).

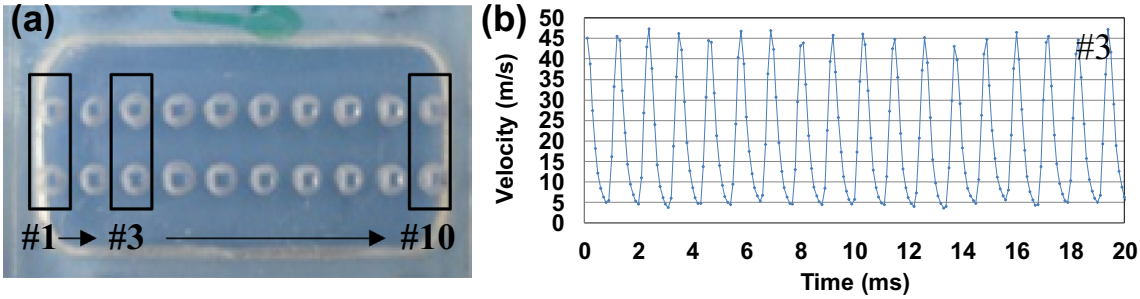

Fig. 4. (a) 20-orifice array with 0.9 mm square orifice and their numbering from left (#1) to right (#10), (b) Instantaneous velocity measurement from orifice location #3.

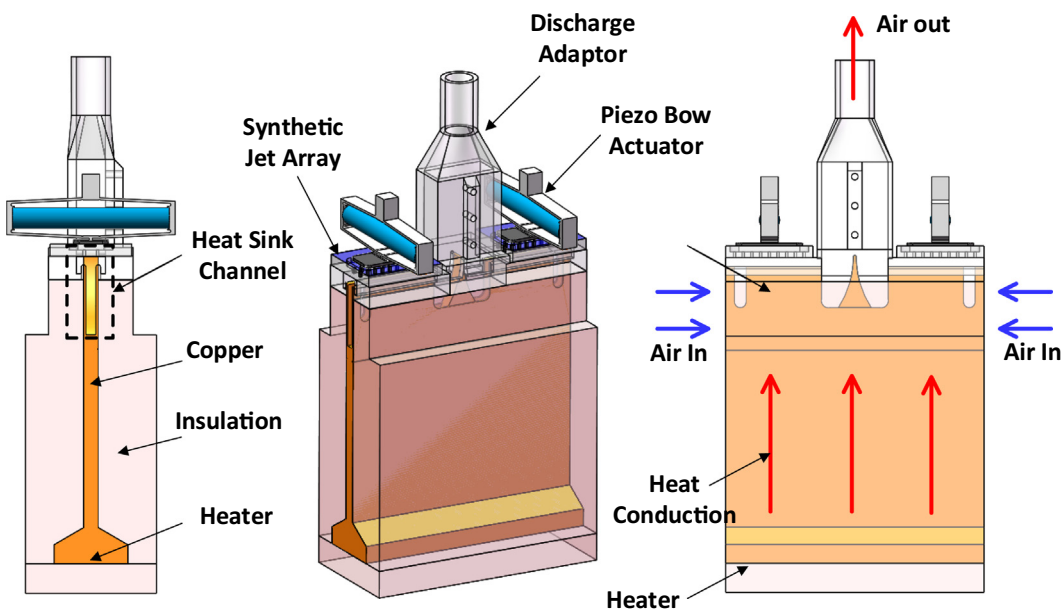

Fig. 5. Test section of single channel heat transfer experiment.

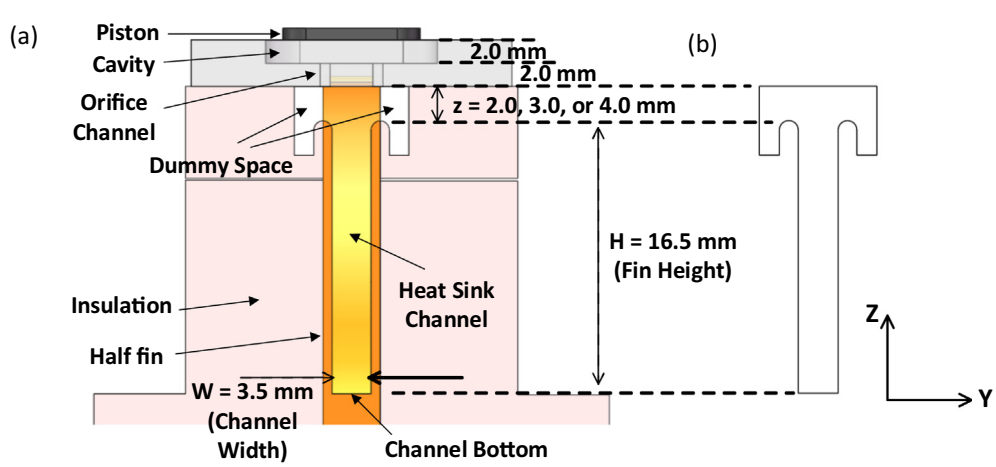

Fig. 6. (a) assembly configuration of channel and synthetic jet, (b) channel cross section for flow passage.

aligned with the centers of the fin tips. The distance between the orifice and fin tip is varied from case to case from 2 mm to 4 mm, with 1 mm increments.

The temperatures along the heat sink channel are measured with E-type, 40-gage thermocouples from OMEGA. The entire single-channel heat sink unit is surrounded with Styrofoam to prevent heat loss to the ambient. Fig. 7 shows the heat transfer experiment set up. An AC signal from a function generator is amplified through a voltage amplifier and transferred to the piezo bow actuators driving the synthetic jet arrays. A vacuum pump is used to draw air through the heat sink channel. Data acquisition and heater control systems are connected to the test section.

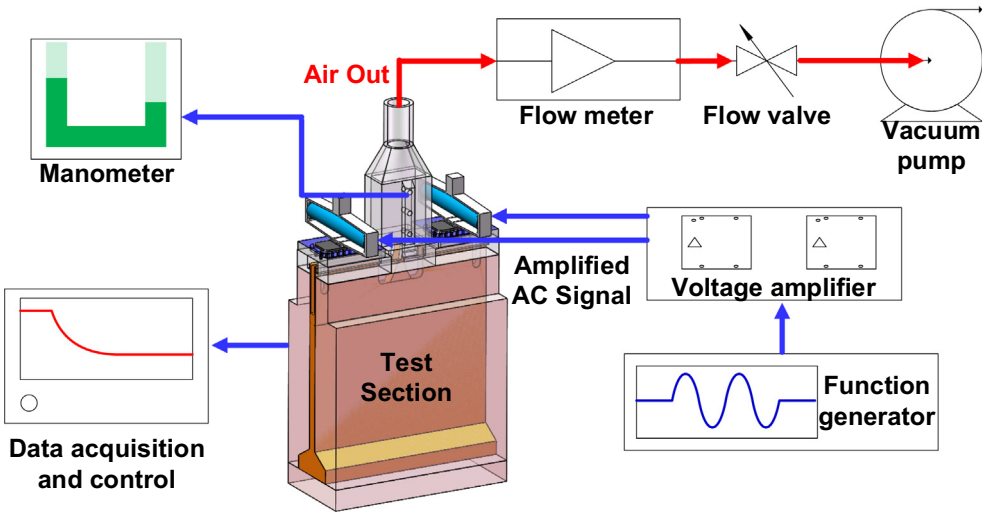

Fig. 7. Schematic of the heat transfer experimental.

2.3. Data reduction and uncertainty analysis

The thermal performance of the single channel heat sink unit was evaluated by obtaining the average convective heat transfer coefficient at the channel surface. The heat transfer coefficient was determined by:

$$h = q/(A_s \times \Delta T_{LMTD}) \tag{1}$$

where A_s is the total fin surface area and q is the thermal energy input, determined by:

$$q = k_c A_c \frac{\Delta T}{\Delta x} \tag{2}$$

where k_c, A_c, and $\Delta T/\Delta x$ are the thermal conductivity of copper, the cross-sectional area of the copper block, and the temperature gradient along the copper block, respectively. The log mean temperature difference, ΔT_{LMTD}, is given by:

$$\Delta T_{LMTD} = \frac{(T_{fin\_in} - T_{air\_in}) - (T_{fin\_out} - T_{air\_out})}{\ln[(T_{fin\_in} - T_{air\_in})/(T_{fin\_out} - T_{air\_out})]} \tag{3}$$

where T_{fin_in}, T_{fin_out} and T_{air_in} are measured temperatures of the fin at the inlet, the fin at the outlet, and the air at the inlet, respectively. The air outlet temperature (T_{air_out}) is calculated by the energy balance between the inlet and outlet of the channel:

$$T_{air\_out} = T_{air\_in} + q/(\rho \cdot c_P \cdot \dot{Q}) \tag{4}$$

where ρ and c_p are air density and air specific heat. The volume flow rate through the channel is $\dot{Q}$. All the measurements are taken after the system reaches steady state. Fig. 8 details the locations of the temperature measurements used in Eqs. (2)–(4).

The uncertainty associated with the heat transfer coefficient measurement was contributed by temperature measurement, thermocouple location and flow rate readings. A 95% confidence interval was used for the uncertainty analysis. The uncertainty in temperature measurement is 0.5 °C. The uncertainty in thermocouple location is 1 mm over a 11.0 mm range. The uncertainty in flow rate is 0.5 L per minute (LPM) over a nominal 66 LPM range. Based on the above uncertainties, the uncertainty of the heat transfer coefficient based on the same confidence interval is 5.6%.

2.4. Results and discussions

The heat transfer experimental results obtained from the single channel test section with the synthetic jet arrays with different orifice shapes are shown in Table 2. The operating conditions of the synthetic jet were 1240 Hz and 100 V. However, the corresponding peak jet velocities of five orifice types should be different due to the discrepancy in their total orifice areas assuming that the mass flow rate generated by the same piston movement is consistent under the same operational condition. The experiments were conducted with a channel flow velocity of 14.7 m/s. The distance from the orifice to the fin tip was maintained to 2 mm. The jet array with the square orifice demonstrated the best heat transfer performance, showing 9.3% enhancement in heat transfer over values for channel through-flow only. The circular and double-slot orifice types followed in the next showing around 7.1–7.4% enhancement in channel heat transfer performance. It is surprised to note that the double-slot showed the similar cooling performance as the circular orifice since the double-slot has about 73% increased total orifice area compared to the circular or square types anticipating reduced jet peak velocity. The split-circular orifice is somewhat obvious falling out showing the minimum heat transfer enhancement even though the peak jet velocity must be kept in the same range as those of circular or square orifices. There seems other dominating factors exist other than the jet peak velocity that affect the heat transfer performance. The explanations from the previous investigation (Pavlova and Amitay [36]) can be adopted to explain the dependency of heat transfer enhancement on different orifice sizes. They explained the frequency and z/d effects on synthetic jet cooling relating to the wavelength and size of the generated vortex ring coherent structures. In the current study, the vortex ring structure created from the split-circular should be smaller than those of circular or square orifices, and therefore may break up into smaller structures before they deliver strong momentum impact on the heated surface providing less heat transfer enhancement. Unsteady characteristics of vortex rings created at the edges of different orifice types should be further examined to unveil the mechanisms of heat transfer enhancement from different configurations of jet orifice. However, under the specific conditions of current experimental study, considering the uncertainty in heat transfer coefficient, the effect of different orifice configurations on heat transfer enhancement is not very significant. The effect of the distance between the orifice and fin tip on thermal performance of the synthetic jet array was investigated with the circular

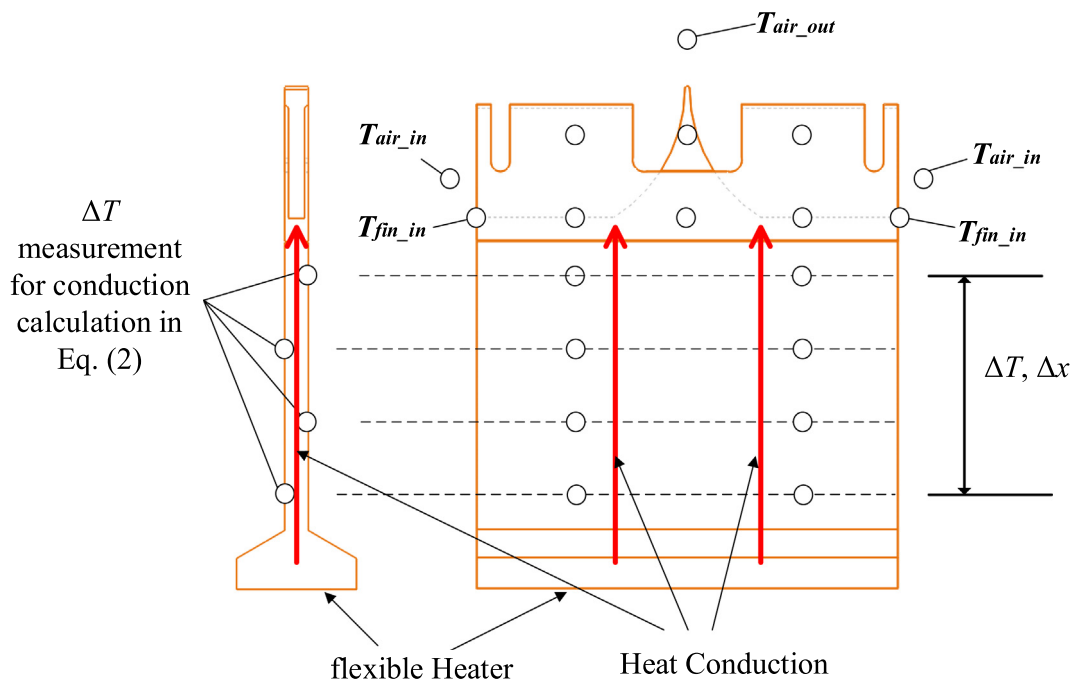

Fig. 8. Detailed locations of temperature measurements for calculations of heat transfer coefficients and heat input.

Table 2
Experimental results of synthetic jet performance with different orifice arrays.

Orifice type		Circular	Split-circular	Square	Double-slot	Inclined
Heat transfer coefficient (W/m^2 K)	Channel flow (14.7 m/s)	156	155	155	160	150
	Channel flow (14.7 m/s) + Syn-Jets (1240 Hz, 100 V)	167	162	170	172	160
Jet contribution		7.1%	4.5%	9.3%	7.4%	6.7%

orifice array with a channel through-flow of 8 m/s, shown in Table 3. The ratio (z/d) of the orifice-to-fin-tip distance (z) and the orifice diameter (d) varied from 2 to 4. As a result, the contribution on heat transfer enhancement from the synthetic jet array increased from 10.0% to 21.7% when z/d decreased from 4 to 2. This is consistent with the previous investigation [36] that the heat transfer enhances as z/d decreases when the jet operating frequency is high. This is owing to the facts that the wavelength and size of the vortex ring structures generated at high operating frequency are small requiring shorter traveling distance before they impact on the heated surface. In comparing the results between Tables 2 and 3, one sees that the synthetic jet contribution on overall heat transfer performance of the channel increases when the velocity of through flow is decreased from 14.7 m/s to 8 m/s using the same z/d of 2.

The baseline experimental results of the channel through-flow-only cases with z/d = 2 in Tables 2 and 3 are validated with empirical relations in the literature. The channel flows of 8.0 m/s and 14.7 m/s investigated fall in turbulent regime based on their Reynolds numbers (2903 and 5079) calculated using the channel hydraulic diameter (D_h) of 5.6 mm. The condition of the entire heat sink channel can be considered as thermally and hydraulically non-fully developed region as the ratio of the channel length (44.5 m) and the hydraulic diameter is smaller than 10 [49]. Based on the channel characteristics evaluated above, the empirical relation from Sleicher and Rouse [50] is used for calculating the average Nusselt number for the channel as:

$$Nu_{avg} = 05 + 0.015Re^{a}Pr^{b} \tag{5}$$

where Re and Pr are the Reynolds number and Prandtl number, respectively. In the above expression, a and b are defined as [50]:

$$a = 0.88 - 0.24/(4 + Pr) \tag{6}$$

$$b = 0.333 + 0.5e^{-0.6Pr} \tag{7}$$

Eq. (5) for the average Nusselt number assumes the flow to be fully developed along the entire channel length. Therefore, a minor correction is made to obtain the average Nusselt number for the non-fully developed (entrance) region of the current experimental condition according to Boelter et al. [51]:

$$Nu_{ent} = Nu_{avg}(1 + 6/(X/D_h)) \tag{8}$$

where Nu_{ent} represents the actual average Nusselt number for the heat sink channel that is maintained as the non-fully developed

Table 3
Heat transfer performance of circular synthetic jet array with different z/d.

z/d		2	3	4
Heat transfer coefficient (W/m^2 K)	Channel flow (8.0 m/s)	115	105	110
	Channel flow (8.0 m/s) + Syn-Jets (1240 Hz, 100 V)	140	123	121
Jet contribution		21.7%	17.1%	10.0%

region. Then, the average heat transfer coefficients of the heat sink channel can be calculated from:

$$h_{avg} = Nu_{ent} k_f / D_h \tag{9}$$

where D_h and k_f are the hydraulic diameter of heat sink flow channel and air thermal conductivity, respectively. The average heat transfer coefficients of the channel calculated based on the Eqs. (5)–(9) for the channel through-flow only conditions of 8.0 m/s and 14.7 m/s are 108.7 W/m^2 K and 149.6 W/m^2 K, respectively. These values agree well with the baseline experimental results shown in Tables 2 and 3 within the error of maximum 7%.

3. Numerical study

3.1. Numerical prediction procedure

The numerical study was conducted to support the experimental study and to further investigate the effects of jet velocity, channel through-flow velocity and z/d on heat transfer performance of synthetic jet impingement on a heat sink channel.

Fig. 9 shows the flow domain for the numerical study, with the boundary conditions indicated. The square orifice configuration (0.9 mm × 0.9 mm) was used for the study, as it showed the best performance in the experiments. For presentation of the results, the fin is divided into two different sections, the fin tip and the fin side surfaces, for documenting the impact of the jets on different locations of the fin. The fin tip is defined as the curved section of the fin structure at its top, as indicated in Fig. 9. The radius of fin tip curvature is 0.8 mm. The remainder of the fin, the straight section, is considered to be the side surface. For the numerical study, average Nusselt numbers were evaluated for the tip, side, and the combined surfaces of the fin as:

$$Nu_{tip} = \frac{h_{tip} D_h}{k_f} \tag{10}$$

$$Nu_{side} = \frac{h_{side} D_h}{k_f} \tag{11}$$

$$Nu_{total} = \frac{h_{total} D_h}{k_f} \tag{12}$$

Average heat transfer coefficients are h_{tip}, h_{side}, and h_{total}, evaluated for the tip, side, and entire surfaces of the fin. The areas for the single fin tip (A_{tip}) and single fin side (A_{side}) surfaces are:

$$A_{tip} = \pi RL \tag{13}$$

$$A_{side} = HL \tag{14}$$

The diaphragm oscillation is realized in ANSYS FLUENT by using a moving-wall boundary condition with a layered dynamic mesh. At different phases of oscillation, the software updates the mesh and computes the governing equations for fluid flow and heat transfer. The inlet of the channel is defined as a uniform velocity boundary condition with a constant air temperature of 27 °C. The value of the inlet velocity is adjusted by matching the flow rates with those of the experiment. All convective heat transfer wall boundary conditions for the fins are defined as no-slip and constant temperature, 37 °C. The pressure-outlet boundary condition is employed. All other walls have the no-slip and adiabatic wall boundary condition. The three-dimensional, incompressible, time-dependent Reynolds-Averaged Navier-Stokes equations (RANS) are solved with the shear-stress-transport (SST), k-ω turbulence model. First-order implicit, and Euler discretization is used for the time model. The second-order upwind scheme is employed

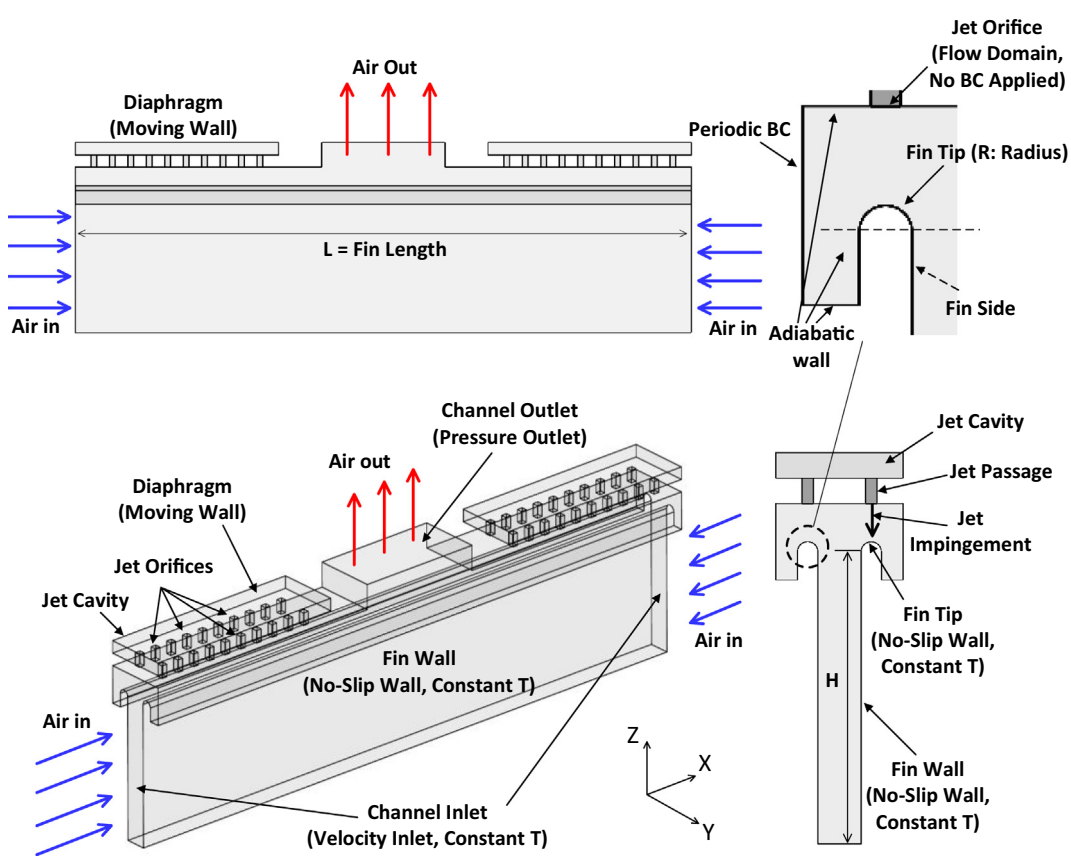

Fig. 9. Flow domain of the numerical simulation, with boundary conditions.

for other terms in the momentum and the energy equations. The Semi-Implicit Method for Pressure Linked Equations (SIMPLE) algorithm is adapted for pressure-velocity field coupling. For each oscillation cycle, the program runs 50 time steps of 1.6×10^{-5} s each and internal iterations continue until the residuals are reduced to 10^{-6}.

3.2. Numerical validation results

One specific series was run with different mesh sizes to validate grid independence and minimize computational error. The results show good convergence with a maximum difference of less than 5% among the different mesh size conditions investigated. Fig. 10 shows a comparison of the heat transfer results between the experiment and numerical simulation in terms of the Nusselt number evaluated over the entire fin surfaces at different z/d values. The channel bulk mean velocity is maintained at 8 m/s. The experimental results show that heat transfer decreases as z increases from 2 mm to 3 mm, then rises as z further increases to 4 mm, whether the jets are activated or not. Since the channel velocity is kept the same, the volume flow rate through the channel must increase as the z value increases. The nonlinearity of heat transfer with changing z value at a fixed channel through-flow velocity (Fig. 10) is not clear. This nonlinearity is not shown from the numerical simulation results. Flow rearrangement in the cooled zone is complex, with local flow separation and reattachment. Overall, the comparison between experiment and simulation shows good agreement, with a maximum difference of less than 10% in average Nusselt number calculated for the total heat transfer surface of the channel wall.

3.3. Parametric study

A parametric study of a synthetic jet array cooling a heat sink channel was performed using the numerical model validated previously. The operating frequency of the synthetic jet was set as 1240 Hz with z = 3 mm. To characterize flow conditions, the Reynolds numbers were defined for both jet and channel flows. The Reynolds number for the synthetic jet is defined as:

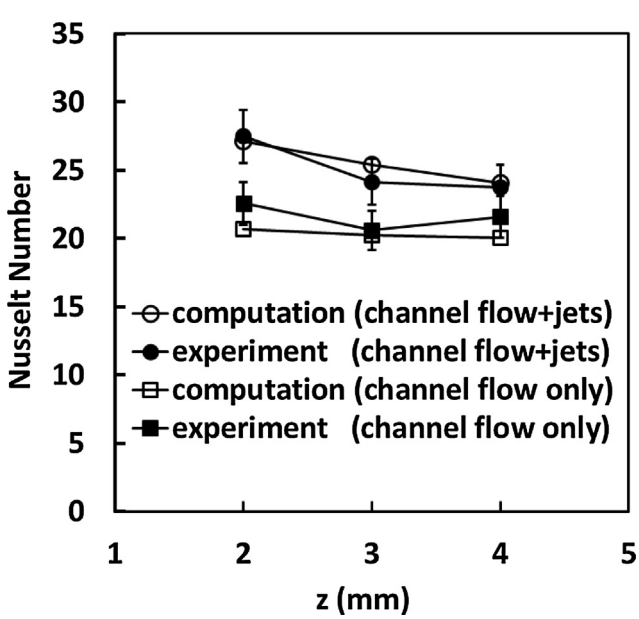

Fig. 10. Comparison of average Nusselt numbers between experiment and simulation.

$$Re\_\text{jet} = \frac{\rho V_j d_h}{\mu} \tag{15}$$

where V_j, d_h, and μ are the jet peak velocity, hydraulic diameter of the jet orifice, and dynamic viscosity of air, respectively. The Reynolds number for the channel flow is:

$$Re\_\text{channel} = \frac{\rho U D_h}{\mu} \tag{16}$$

Herein, U and D_h are the average velocity of channel through-flow and hydraulic diameter of the heat sink channel, respectively. Conditions of the channel through-flow and synthetic jet impingement flow are summarized in terms of their channel mean flow velocities and jet maximum velocities in Table 4.

3.3.1. Jet effects

Fig. 11 shows the average Nusselt numbers calculated by changing both *Re*_jet and *Re*_channel for the fin tip, side walls, and entire surface. The Reynolds number, *Re*_jet, ranges from zero to 3715, which correspond to peak jet velocities from 0 m/s to 60 m/s. The peak velocity is attained by controlling the amplitude of the diaphragm motion while maintaining an operating frequency of 1240 Hz. Overall, the heat transfer coefficients at both fin tip and side surfaces improve as *Re*_jet increases at a fixed z value of 3 mm. At the fin tip surface, an increase of 413% in average Nusselt number was observed with a peak jet velocity of 60.3 m/s (*Re*_jet = 3715) over values for the channel-through-flow-only case (*Re*_jet = 0) under the same channel through-flow condition of *Re*_channel = 1451. The channel side surfaces increase about 60% in average Nusselt number over values for the channel-flow-only case, under the same channel flow and synthetic jet conditions. Thus, the fin tip is more sensitive to impinging jet cooling than are the side surfaces. The fin tip is nearer the orifices from which the jets discharge.

When *Re*_jet is over 1000 (V_j = 16 m/s) the synthetic jet impingement on the fin tip is strong and exceeds the channel through-flow cooling effects. As *Re*_channel further increases, enhanced heat transfer on the fin side walls by the impinging jet decreases. When *Re*_channel = 5805 (U = 16 m/s), the synthetic jet with the peak velocity of 60 m/s improves heat transfer only around 11%, over the channel through-flow-only condition. Whereas, at *Re*_channel = 1451 (U = 4 m/s), the synthetic jet improves heat transfer from the side walls by around 83%, over the channel through-flow-only condition. The average Nusselt numbers calculated for the entire fin surface follow the trend of the side walls since the side wall area is much larger than the fin tip area. In summary, the influence of the synthetic jets was found to be mainly near the fin tip region and heat transfer enhancement is higher under lower channel through-flow velocity conditions. The channel through-flow plays as a resistance for the vortex ring structures created from the orifice edges to travel until they reach the heated surfaces. In addition, the channel flow should have an impact on the propagation characteristics of vortex rings and their corresponding heat transfer enhancement mechanisms. Further intensive studies are required to understand phenomena behind these.

3.3.2. Channel flow effects

In this section, the average Nusselt numbers for the fin surfaces are obtained by varying the channel through-flow velocity (U = 4–16 m/s, *Re*_channel = 1451–5805) while fixing the operating conditions of the synthetic jet (Fig. 12). As seen in the previous section, heat transfer in the tip region is found to be less sensitive to changes of channel velocity, except in cases with low *Re*_jet values. One possible reason is that the synthetic jet plays a dominant role when its velocity is large compared to the channel through-flow

Table 4
The conditions of channel flow and synthetic jet impingement used in numerical study.

Channel flow	Velocity (m/s)	0	4	8	12	16			
	*Re*_channel	0	1451	2903	4354	5805			
Synthetic jet	Velocity (m/s)	0	8.7	17.4	26.1	34.8	43.6	51.7	60.3
	*Re*_jet	0	536	1072	1608	2144	2686	3185	3715

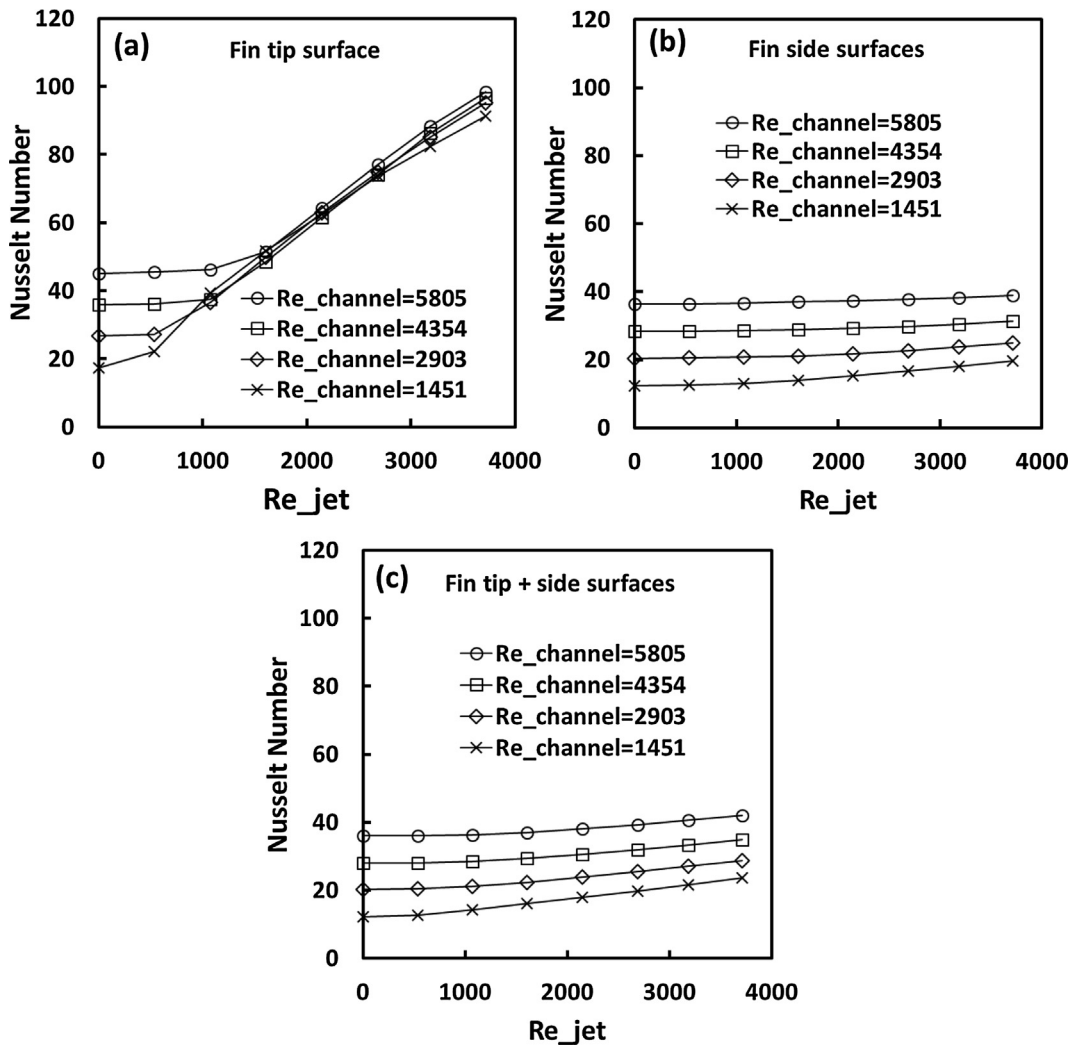

Fig. 11. Average Nusselt number changes with the *Re*_jet: (a) for fin tip; (b) for fin side surface; and (c) for entire fin surface.

velocity. In this case, the created vortex ring structures have stronger momentum to travel through the channel through-flow and reach the fin tip surface. However, when the jet is relatively weak the impinged vortex rings are easily carried away in the channel through-flow before they reach the heated surfaces. This phenomena should become more obvious on the side surfaces of the fin as they are further distanced away from the jet orifices than the fin tip surfaces. The heat transfer on the side walls is found to be more sensitive to increases of channel flow velocity. In the current configuration of the numerical study, the jet is oriented perpendicular to the channel through-flow relating each other to create large resistance. The engaging angle between two components, their operating conditions, and their dimensions may have a significant impact on the characteristics of vortex generation, propagation, and its secondary behavior that can alter heat transfer performance of the channel. In the previous section of the experimental study, the inclined orifice with 60 degrees angle was tested and showed a similar heat transfer performance compared to non-inclined orifice of circular shape. It may be helpful to further investigate the effects of angle, jet operating frequency, and channel through-flow velocity on the channel heat transfer.

3.3.3. z/d effects

A numerical study was conducted to investigate the effects of z on synthetic jet cooling in the heat sink channel. Average Nusselt numbers on the fin surfaces are presented (Fig. 13). The z value is varied from 1 mm to 3 mm while the channel bulk flow is kept at a low velocity of 4 m/s. The jet Reynolds number, *Re*_jet, is varied from zero to 3715 by changing the amplitude of the diaphragm at a fixed jet frequency of 1240 Hz. The trends of heat transfer enhancement on both fin tip and side surfaces show the same pattern; that the heat transfer increases as the z value decreases. Again, this is already anticipated and matches well with previous investigations [36]. This trend becomes even more obvious at

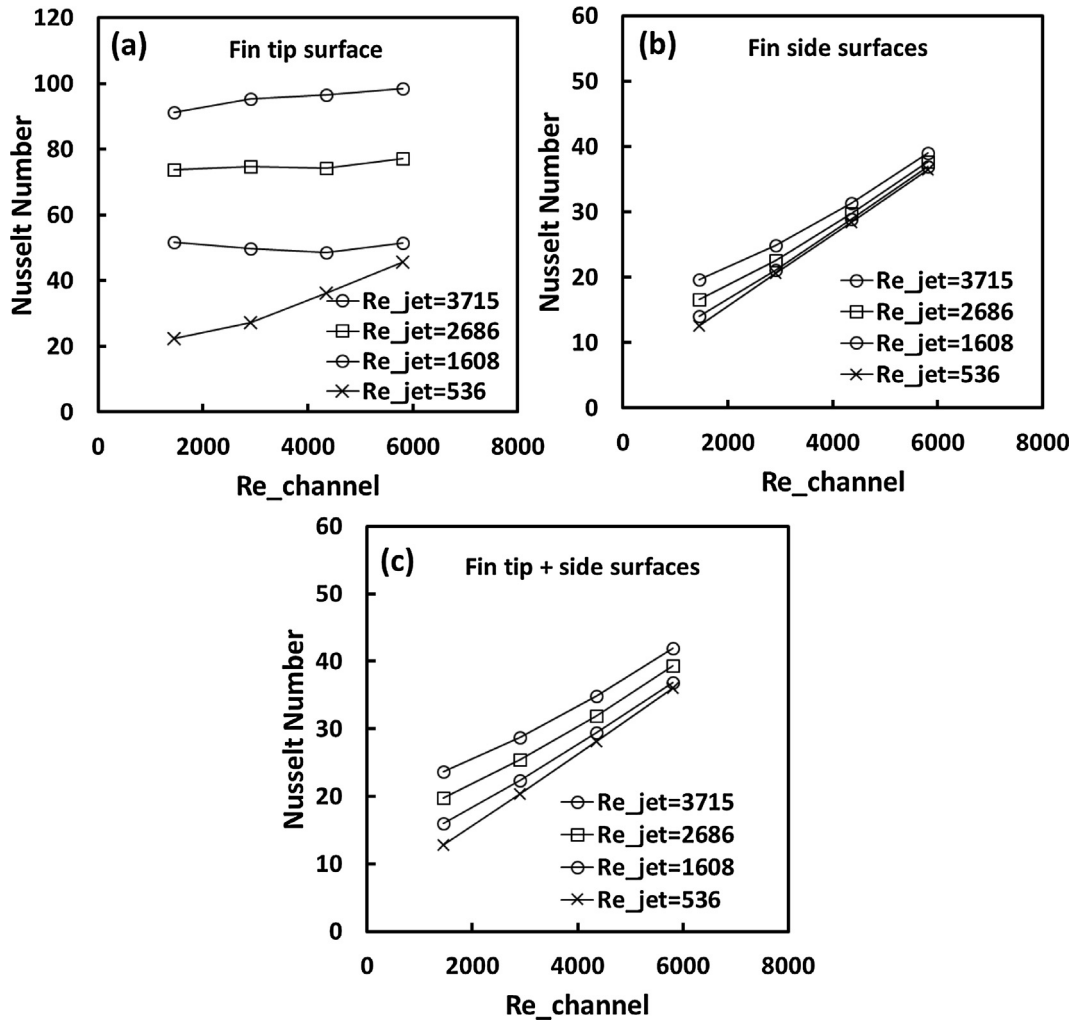

Fig. 12. Average Nusselt number variations with variations of *Re*_channel: (a) for fin tip surface; (b) for fin side surface; and (c) for entire fin surface.

higher jet velocities showing larger heat transfer enhancement at both the fin tip and side surfaces. Overall, heat transfer at the fin tip is more sensitive to changes of z/d value as it is closer to the jet orifices providing shorter distance for the vortex rings to travel before they break up and dissipate in the channel flow. The synthetic jet flow can be more influential on overall heat transfer performance in the heat sink channel if the jet is closer to the fin surface, for it is less likely to be carried away by the channel flow.

4. Summary and conclusions

Heat transfer enhancement using synthetic jet arrays in a single channel of an air-cooled heat sink was investigated experimentally and computationally. A heat transfer test facility was fabricated to measure heat transfer coefficients on the fin surfaces. The synthetic jet array assembly was driven by a piezo-bow actuator that operates at a frequency of 1240 Hz at 100 V. Five different orifice types of circular, split-circular, square, double-slots, and inclined were fabricated to investigate the effects of orifice shape on heat transfer enhancement of the channel. The circular orifice with 1 mm diameter generated a peak jet velocity of around 45 m/s. The square orifice showed the maximum heat transfer enhancement of around 9.3% over the channel through-flow only case of 14 m/s at z = 2 mm. The effects of different orifice shapes must be related to the unsteady characteristics of vortex ring structures generated from them regarding their propagation and dissipation. Although the effects of the orifice shape were not significant in the specific conditions of the current experimental study, further investigations are recommended to clearly understand the phenomena behind them. When the channel through-flow velocity was reduced to 8 m/s, the circular orifice provided a heat transfer enhancement of 21.7% at z = 2 mm. The heat transfer enhancement further decreased as z value increased. This trend matches with the previous investigation in the literature. A numerical model was first validated by comparing its results to the experimental data. It was then used for performing a parametric study to see the effects of synthetic jet and channel flow velocities. It was found that heat transfer in the fin tip region is more sensitive to synthetic jet impingement due to the closer distance to the jet orifices that helps the generated vortex ring structures to reach more effectively. Maximum average heat transfer enhancement of around 413% was found from the fin tip region by turning on the synthetic jet arrays at 1240 Hz with a channel flow of 4 m/s velocity. The channel flow was found to be more effective than the jet in cooling the fin side surfaces. Finally, a study performed to understand the effects of distance between the jet orifice and the fin tip showed

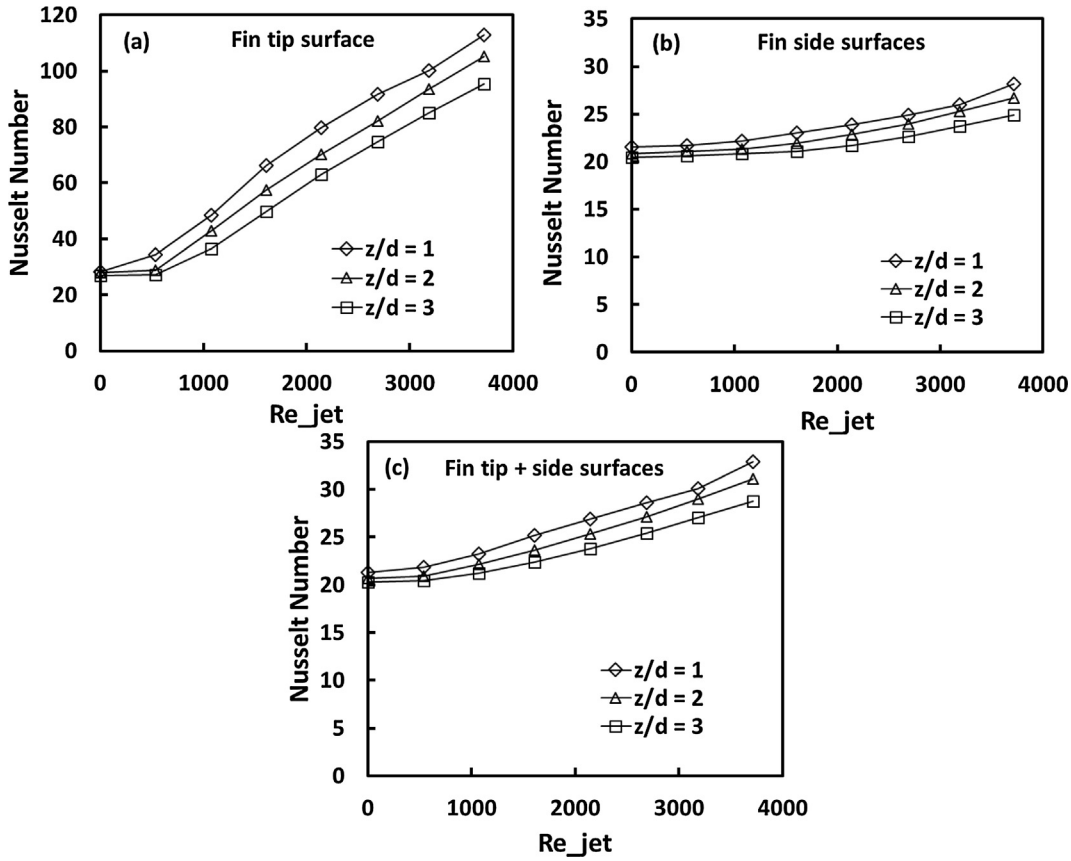

Fig. 13. Average Nusselt numbers with different z/d values: (a) for fin tip surface; (b) for fin side surfaces; and (c) for entire fin surface.

that synthetic jets can be more effective in cooling the fin tip when the separation distance is small. This trend matches with the experimental results showed in the current study as well as previous investigation in the literature.

Declaration of Competing Interest

There is no conflict of interest in this paper.

Acknowledgements

This work was partially supported by the Defense Advanced Research Projects Agency (DARPA) MACE Program. The views expressed are those of the authors and do not reflect the official policy or position of the Department of Defense or the U.S. Government. Approved for Public Release, Distribution Unlimited. The computational part of this work was supported by the Minnesota Supercomputing Institute (MSI) computation resources.

References

[1] A. Miner, U. Ghoshal, Cooling of high-power-density microdevices using liquid metal coolants, Appl. Phys. Lett. 85 (3) (2004) 506–508.
[2] C.S. Sharma, M.K. Tiwari, S. Zimmermann, T. Brunschwiler, G. Schlottig, B. Michel, D. Poulikakos, Energy efficient hotspot-targeted embedded liquid cooling of electronics, Appl. Energy 138 (2015) 414–422.
[3] P. Foroughi, V. Benetis, M. Ohadi, Y. Zhao, J. Lawler, Design, testing and optimization of a micropump for cryogenic spot cooling applications, in: Semiconductor Thermal Measurement and Management IEEE Twenty First Annual IEEE Symposium, 2005, 2005, pp. 335–340.
[4] E. Jiaqiang, D. Han, A. Qiu, H. Zhu, Y. Deng, J. Chen, X. Zhao, W. Zuo, H. Wang, J. Chen, Q. Peng, Orthogonal experimental design of liquid-cooling structure on the cooling effect of a liquid-cooled battery thermal management system, Appl. Therm. Eng. 132 (2018) 508–520.
[5] U. Ghoshal, D. Grimm, S. Ibrani, C. Johnston, A. Miner, High-performance liquid metal cooling loops, in: Semiconductor Thermal Measurement and Management IEEE Twenty First Annual IEEE Symposium, 2005, 2005, pp. 16–19.
[6] C.T. Nguyen, G. Roy, C. Gauthier, N. Galanis, Heat transfer enhancement using Al_2O_3–water nanofluid for an electronic liquid cooling system, Appl. Therm. Eng. 27 (8) (2007) 1501–1506.
[7] S.M. Peyghambarzadeh, S.H. Hashemabadi, S.M. Hoseini, M. Seifi Jamnani, Experimental study of heat transfer enhancement using water/ethylene glycol based nanofluids as a new coolant for car radiators, Int. Commun. Heat Mass Transf. 38 (9) (2011) 1283–1290.
[8] M.A. Chan, C.R. Yap, K.C. Ng, Modeling and testing of an advanced compact two-phase cooler for electronics cooling, Int. J. Heat Mass Transf. 52 (15) (2009) 3456–3463.
[9] S. Myung Ki, I. Mudawar, Single-phase and two-phase hybrid cooling schemes for high-heat-flux thermal management of defense electronics, in: 2008 11th Intersociety Conference on Thermal and Thermomechanical Phenomena in Electronic Systems, 2008, pp. 121–131.
[10] K.P. Drummond, D. Back, M.D. Sinanis, D.B. Janes, D. Peroulis, J.A. Weibel, S.V. Garimella, A hierarchical manifold microchannel heat sink array for high-heat-flux two-phase cooling of electronics, Int. J. Heat Mass Transf. 117 (2018) 319–330.
[11] X.F. Peng, B.X. Wang, Forced convection and flow boiling heat transfer for liquid flowing through microchannels, Int. J. Heat Mass Transf. 36 (14) (1993) 3421–3427.
[12] J. Linan, W. Man, Y. Zohar, Phase change in microchannel heat sinks with integrated temperature sensors, J. Microelectromech. Syst. 8 (4) (1999) 358–365.
[13] M. Visaria, I. Mudawar, Application of two-phase spray cooling for thermal management of electronic devices, IEEE Trans. Compon. Packag. Technol. 32 (4) (2009) 784–793.
[14] L. Lin, R. Ponnappan, Heat transfer characteristics of spray cooling in a closed loop, Int. J. Heat Mass Transf. 46 (20) (2003) 3737–3746.
[15] S.M. You, T.W. Simon, A. Bar-Cohen, A technique for enhancing boiling heat transfer with application to cooling of electronic equipment, IEEE Trans. Compo. Hybr. Manuf. Technol. 15 (5) (1992) 823–831.
[16] I. Mudawar, Direct-immersion cooling for high power electronic chips, in: [1992 Proceedings] Intersociety Conference on Thermal Phenomena in Electronic Systems, 1992, pp. 74–84.
[17] S.M. You, J.H. Kim, K.H. Kim, Effect of nanoparticles on critical heat flux of water in pool boiling heat transfer, Appl. Phys. Lett. 83 (16) (2003) 3374–3376.

[18] M. Behnia, D. Copeland, D. Soodphakdee, A comparison of heat sink geometries for laminar forced convection: numerical simulation of periodically developed flow, in: ITherm'98. Sixth Intersociety Conference on Thermal and Thermomechanical Phenomena in Electronic Systems (Cat. No.98CH36208), 1998, pp. 310–315.
[19] T. Meng-Chang, K. Shung-Wen, L. Chih-Hsien, A novel copper bead heat sink for computer cooling, in: 2009 25th Annual IEEE Semiconductor Thermal Measurement and Management Symposium, 2009, pp. 228–231.
[20] C. Hilbert, S. Sommerfeldt, O. Gupta, D.J. Herrell, High performance air cooled heat sinks for integrated circuits, IEEE Trans. Compo. Hybr. Manuf. Technol. 13 (4) (1990) 1022–1031.
[21] C.L. Chapman, S. Lee, B.L. Schmidt, Thermal performance of an elliptical pin fin heat sink, in: Proceedings of 1994 IEEE/CHMT 10th Semiconductor Thermal Measurement and Management Symposium (SEMI-THERM), 1994, pp. 24–31.
[22] A. Bhattacharya, R.L. Mahajan, Finned metal foam heat sinks for electronics cooling in forced convection, J. Electron. Packag. 124 (3) (2002) 155–163.
[23] D. Kim, S.J. Kim, A. Ortega, Compact modeling of fluid flow and heat transfer in pin fin heat sinks, J. Electron. Packag. 126 (3) (2004) 342–350.
[24] S.M. Wait, S. Basak, S.V. Garimella, A. Raman, Piezoelectric fans using higher flexural modes for electronics cooling applications, IEEE Trans. Compon. Packag. Technol. 30 (1) (2007) 119–128.
[25] J. Petroski, M. Arik, M. Gursoy, Optimization of piezoelectric oscillating fan-cooled heat sinks for electronics cooling, IEEE Trans. Compon. Packag. Technol. 33 (1) (2010) 25–31.
[26] M. Kimber, S.V. Garimella, A. Raman, Local heat transfer coefficients induced by piezoelectrically actuated vibrating cantilevers, J. Heat Transf. 129 (9) (2007) 1168–1176.
[27] S.-F. Liu, R.-T. Huang, W.-J. Sheu, C.-C. Wang, Heat transfer by a piezoelectric fan on a flat surface subject to the influence of horizontal/vertical arrangement, Int. J. Heat Mass Transf. 52 (11) (2009) 2565–2570.
[28] P. Burmann, A. Raman, S.V. Garimella, Dynamics and topology optimization of piezoelectric fans, IEEE Trans. Compon. Packag. Technol. 25 (4) (2002) 592–600.
[29] B.L. Owsenek, J. Seyed-Yagoobi, R.H. Page, Experimental investigation of corona wind heat transfer enhancement with a heated horizontal flat plate, J. Heat Transf. 117 (2) (1995) 309–315.
[30] M. Molki, K.L. Bhamidipati, Enhancement of convective heat transfer in the developing region of circular tubes using corona wind, Int. J. Heat Mass Transf. 47 (19) (2004) 4301–4314.
[31] T. Yeom, T.W. Simon, L. Huang, M.T. North, T. Cui, Piezoelectric translational agitation for enhancing forced-convection channel-flow heat transfer, Int. J. Heat Mass Transf. 55 (25) (2012) 7398–7409.
[32] T. Yeom, T.W. Simon, Y. Yu, M.T. North, T. Cui, Convective Heat Transfer Enhancement on a Channel Wall With a High Frequency, Oscillating Agitator, in: ASME International Mechanical Engineering Congress and Exposition, ASME, Denver, USA, 2011, pp. 875–884.
[33] T. Yeom, T.W. Simon, M. North, T. Cui, High-frequency translational agitation with micro pin-fin surfaces for enhancing heat transfer of forced convection, Int. J. Heat Mass Transf. 94 (2016) 354–365.
[34] M. Chaudhari, B. Puranik, A. Agrawal, Heat transfer characteristics of synthetic jet impingement cooling, Int. J. Heat Mass Transf. 53 (5) (2010) 1057–1069.
[35] M. Chaudhari, B. Puranik, A. Agrawal, Effect of orifice shape in synthetic jet based impingement cooling, Exp. Therm Fluid Sci. 34 (2) (2010) 246–256.
[36] A. Pavlova, M. Amitay, Electronic cooling using synthetic jet impingement, J. Heat Transf. 128 (9) (2006) 897–907.
[37] J. Garg, M. Arik, S. Weaver, T. Wetzel, S. Saddoughi, Meso scale pulsating jets for electronics cooling, J. Electron. Packag. 127 (4) (2005) 503–511.
[38] Y. Utturkar, M. Arik, C.E. Seeley, M. Gursoy, An experimental and computational heat transfer study of pulsating jets, J. Heat Transf. 130 (6) (2008), 062201-062201-062210.
[39] M. Arik, Local heat transfer coefficients of a high-frequency synthetic jet during impingement cooling over flat surfaces, Heat Transf. Eng. 29 (9) (2008) 763–773.
[40] D. Jagannatha, R. Narayanaswamy, T.T. Chandratilleke, Analysis of a synthetic jet-based electronic cooling module, Numer. Heat Transf. Part A Appl. 56 (3) (2009) 211–229.
[41] B.L. Smith, A. Glezer, The formation and evolution of synthetic jets, Phys. Fluids 10 (9) (1998) 2281–2297.
[42] T.T. Chandratilleke, D. Jagannatha, R. Narayanaswamy, Performance analysis of a synthetic jet-microchannel hybrid heat sink for electronic cooling, in: 2009 11th Electronics Packaging Technology Conference, 2009, pp. 630–635.
[43] R.C. Behera, P. Dutta, K. Srinivasan, Numerical study of interrupted impinging jets for cooling of electronics, IEEE Trans. Compon. Packag. Technol. 30 (2) (2007) 275–284.
[44] N. Erbas, O. Baysal, Micron-Level Actuators for Thermal Management of Microelectronic Devices (4272X) (2007) 219–228.
[45] A. Terzis, G. Wagner, J. von Wolfersdorf, P. Ott, B. Weigand, Hole staggering effect on the cooling performance of narrow impingement channels using the transient liquid crystal technique, J. Heat Transf. 136 (7) (2014), 071701-071701-071709.
[46] A. Terzis, P. Ott, J. von Wolfersdorf, B. Weigand, M. Cochet, Detailed heat transfer distributions of narrow impingement channels for cast-in turbine airfoils, J. Turbomach. 136 (9) (2014), 091011-091011-091019.
[47] T. Yeom, T.W. Simon, M. Zhang, M.T. North, T. Cui, High frequency, large displacement, and low power consumption piezoelectric translational actuator based on an oval loop shell, Sens. Actuat. A 176 (2012) 99–109.
[48] T. Yeom, T. Simon, M. Zhang, Y. Yu, T. Cui, Active heat sink with piezoelectric translational agitators, piezoelectric synthetic jets, and micro pin fin arrays, Exp. Therm Fluid Sci. 99 (2018) 190–199.
[49] F.P. Incropera, D.P. Dewitt, T.L. Bergman, A.S. Lavine, Fundamentals of Heat and Mass Transfer, sixth ed. Wiley.
[50] C.A. Sleicher, M.W. Rouse, A convenient correlation for heat transfer to constant and variable property fluids in turbulent pipe flow, Int. J. Heat Mass Transf. 18 (5) (1975) 677–683.
[51] L.M.K. Boelter, G. Young, H.W. Iversen, An Investigation of Aircraft Heaters XXVII: Distribution of Heat-transfer Rate in the Entrance Section of a Circular Tube, 1948.